

Precision measurements of large scale structure with future type Ia supernova surveys

Steen Hannestad, Troels Haugbølle, Bjarne Thomsen

Department of Physics and Astronomy, University of Aarhus, Ny Munkegade,
DK-8000 Aarhus C, Denmark

E-mail: sth@phys.au.dk

Abstract. Type Ia supernovae are currently the best known standard candles at cosmological distances. In addition to providing a powerful probe of dark energy they are an ideal source of information about the peculiar velocity field of the local universe. Even with the very small number of supernovae presently available it has been possible to measure the dipole and quadrupole of the local velocity field out to $z \sim 0.025$. With future continuous all-sky surveys like the LSST project the luminosity distances of tens of thousands of nearby supernovae will be measured accurately. This will allow for a determination of the local velocity structure of the universe as a function of redshift with unprecedented accuracy, provided the redshifts of the host galaxies are known. Using catalogues of mock surveys we estimate that future low redshift supernova surveys will be able to probe σ_8 to a precision of roughly 5% at 95% C.L. This is comparable to the precision in future galaxy and weak lensing surveys and with a relatively modest observational effort it will provide a crucial cross-check on future measurements of the matter power spectrum.

1. Introduction

Precision measurements of distant type Ia supernovae have been an essential ingredient in building the present standard model of cosmology in which the energy density of the universe is dominated by dark energy [1–3]. The main interest so far has been in supernovae in the redshift range 0.5–1.5 [4–9], which corresponds to the transition region between matter and dark energy domination.

However, there is a rapidly increasing interest in supernovae at much lower redshifts [10–15]. The low redshift supernovae provide an anchor for the Hubble diagram which is important for the determination of dark energy parameters. Since they are much brighter they are also useful as a laboratory for calibrating the relation between the supernova light curve shape and its inherent brightness.

A potentially even more interesting feature of low redshift supernovae is that the velocity field associated with the large scale structure of the universe is imprinted on the apparent magnitudes and redshifts of the supernovae. If this is not corrected for it will lead to relatively large and correlated errors in the measured luminosity distance of low redshift supernovae, a potentially serious source of error for future dark energy surveys [10, 12, 14, 16, 17]. However, the velocity field can also be used to probe the local large scale structure of the universe.

With the current fairly small datasets at low redshift only the local dipole [18, 19] and quadrupole [11] terms in the velocity field have been measured (see also [15]), and agree with other types of flow measurements. These preliminary studies, however, clearly demonstrate the potential of using type Ia supernovae for this purpose. The very small intrinsic scatter in luminosity means that the local velocity field can be measured as precisely with ~ 100 supernovae as with an order of magnitude more galaxies used as standard candles.

In the present work we will, for the first time, study how future type Ia supernova measurements can be used for detailed studies of the large scale structure of the universe. It turns out that the large scale velocity power spectrum can be measured quite precisely using around 10^5 supernovae, a number which will be observed with surveys such as the Large Synoptic Survey Telescope (LSST) [20].

In order to investigate the potential of such future measurements we use detailed mock supernova catalogues produced from high resolution N-body simulations. We find that the survey strategy for measuring the supernovae is very important and investigate this phenomenon in detail.

Our most important finding is that future supernova surveys can be used to probe cosmological parameters such as σ_8 , the amplitude of fluctuations on small scales, at a precision which is competitive with other future cosmological probes.

In Section 2 we present the assumed supernova rates and discuss upcoming surveys in this context. Section 3 provides a review of the velocity power spectrum, as well as a simple method for analytically calculating the angular velocity power spectrum as a function of redshift. Details of the simulations and the power spectrum extraction are

provided in Section 4. The extraction of cosmological parameters from our simulated data sets is discussed in Section 5, and finally Section 6 contains our conclusions.

2. The supernova rate and future surveys

The local type Ia supernova rate is roughly [21–23]

$$R \simeq 1.2_{-1}^{+2} \times 10^{-4} \text{ yr}^{-1} h^3 \text{ Mpc}^{-3}, \quad (1)$$

and while there is considerable uncertainty about the exact rate (see e.g. [24] for a 3 times higher rate deduced using SNfactory data), we will adopt the above rate. If the actual rate is lower (higher) then simply a longer (shorter) survey time would be needed to reach the same number of measured supernovae.

Out to a redshift of z_{\max} , where $z_{\max} \ll 1$ the total number of supernovae per time is then

$$N = 1.3 \times 10^4 \left(\frac{z_{\max}}{0.1} \right)^3 \text{ yr}^{-1} \quad (2)$$

To probe the velocity structure on different length scales, we will analyse the Supernovae in redshift bins. We compare with theory by calculating the angular power spectrum, C_l , in each redshift bin.

As will be seen below, using upcoming surveys and collecting data in a three-year period, taking a conservative approach, the maximum multipole which can be probed at $z < 0.13$ is $l_{\max} \sim 20$. However, the number of supernovae in a bin increases cubically, while the error on individual supernovae δv_r increases linearly with distance. The overall error goes like $\delta v_r/N_{\text{bin}}^{1/2}$ or $z^{-1/2}$, and therefore the precision, that the radial velocity of a given *angular* scale can be measured by, increases with distance.

We also note that exactly because the effective error scales like $\delta v_r/N_{\text{bin}}^{1/2}$, an improved understanding of the light curve–absolute magnitude relation, and environmental effects, such as dust extinction could dramatically decrease the error on the angular power spectrum, compared to what is forecasted in this paper. Such a decrease is not unreasonable to expect, given the much larger and more homogeneous sample of low redshift type Ia supernovae that will be available in the near future.

2.1. Future surveys

Several upcoming surveys will map large portions of the sky at regular intervals to look for either transient sources or hitherto undiscovered solar system objects. In the near future there will be projects such as Pan-STARRS [25] and SkyMapper [26], and in about 2013 the LSST project [20] will start.

The scan strategy of these surveys is not necessarily optimised to search for nearby supernovae, while all of them have dedicated programs for intermediate or high redshift supernovae. Despite this, with the LSST a very large fraction of all type Ia supernovae out to redshifts of order 0.2 will be detected and their light curves measured in detail.

However, since none of these experiments will perform follow-up spectroscopy of the host galaxy, this task will have to be undertaken using other telescopes. Fortunately the host galaxies will usually be sufficiently bright for spectroscopy even with modest sized telescopes, and the task is therefore not unmanageable. We note that a sufficiently accurate spectrum can be obtained in roughly 20 minutes using a 1m class telescope \ddagger , and thousands of redshifts per year can therefore be measured relatively easily using just a few such telescopes. We also note that the important part of the spectroscopy is to determine the redshift of the host galaxy, not the supernova, and that the spectroscopic observations can therefore in principle be done long after the supernova event itself.

Of course this is true only if the supernova can be determined to be a type Ia from the light curve measurements alone with very close to 100% efficiency. With a precise light curve for a supernova in 6 filters sampled every fourth night in a rolling search, it should be possible to reliably detect if it is a type Ia supernova using only photometry [27, 28], and determine the luminosity distance very precisely.

In the following we will assume full sky coverage and use numbers corresponding to the total number of supernovae occurring in three years (assuming the rate given in Eq. 1). If the number of supernovae is lower the numbers can easily be scaled to a longer observation period. Full sky coverage is not essential as long as it is significantly larger than 0.5, and the unobserved area is distributed in at most a few large patches, as is also true for CMB observations.

3. The angular velocity power spectrum

In order to make the analysis of large scale velocity flows simpler we will work with the angular velocity power spectrum. This in turn also makes the extraction of cosmological parameters from the synthetic data easier. Following [29, 30] the angular velocity power spectrum can be simply related to the matter power spectrum in the linear limit. The continuity equation of mass relate the velocity and density: $\nabla \cdot \mathbf{v} = -a\partial\delta/\partial t$. Fourier transforming it, we get

$$\mathbf{k} \cdot \mathbf{v}_k = -iHf(\Omega)\delta_k, \quad (3)$$

where $\delta_{\mathbf{k}}$ is the Fourier transform of the density contrast, and $f(\Omega) = d \log \delta / d \log a \sim \Omega_m^{0.6}$ is the velocity growth factor [31].

The peculiar velocities are measured as averaged quantities over a certain scale. For example the peculiar velocity derived from observing a supernova, and the host galaxy redshift, is the smoothed velocity on the scale of the host galaxy. Likewise, in a N-body simulation the velocity field is measured using a smoothing kernel. Therefore the power spectrum, be it synthetic or observed, is smoothed by a window function, and related to the matter power spectrum as

$$P_v(k) = H^2 f(\Omega)^2 k^{-2} P_m(k) |W(kR)|^2 \quad (4)$$

\ddagger Based on an assumed accuracy of $100 \times (z/0.05)$ km s $^{-1}$ and a redshift of ~ 0.1 .

where $W(kR)$ is the Fourier transform of the window function.

What we are measuring is the angular power spectrum of the radial peculiar velocities on a shell. It can be related to the 3D velocity power spectrum as [29]

$$C_l = \frac{4\pi}{2l+1} (l\mathcal{B}_{l-1} + (l+1)\mathcal{B}_{l+1}), \quad (5)$$

where

$$\mathcal{B}_l = 4\pi \int \frac{k^2 dk}{(2\pi)^3} P_v(k) j_l(kx)^2, \quad (6)$$

$j_l(kx)$ is the spherical Bessel function, and x is the comoving distance to the shell. Figure 1 shows the analytic angular power spectra at different distances compared to the power spectra obtained by directly finding the radial velocity field averaged over different observers in a large scale N-body simulation. There is an excellent agreement between the synthetic spectra and the model for small l , while at large l the discrepancy is due to the assumption of a linear power spectrum, and no shell crossing in Fourier space.

To be consistent with the N-body simulation the radial velocity field in the simulation is determined by smoothing the radial velocities of the particles with the same adaptive smoothing kernel of Monaghan and Lattanzio [32] with 33 neighbours that is used in the simulation. The form of the window function for this smoothing kernel is not a priori clear, since the kernel size is adaptive and varies with density. Therefore one cannot just Fourier transform the kernel with a fixed R . Nonetheless we have found empirically that

$$|W(kR)|^2 = \frac{1}{1+kR}, \quad (7)$$

$$R = 2L_{box} \left(\frac{N_{neighbour}}{N_{particles}} \right)^{1/3} \quad (8)$$

is an excellent approximation. Here L_{box} is the box size, $N_{particles}$ the number of particles in the simulation, and $N_{neighbour}$ the number of neighbour particles used in the smoothing process.

The analytic matter power spectrum $P_m(k)$ is a standard linear matter power spectrum with $(h, \Omega_m, \Omega_\Lambda, \sigma_8) = (0.7, 0.3, 0.7, 0.9)$ computed using CAMB [33].

3.1. Analytic Approximation

From Eq. 5 we see that the velocity angular power spectrum is related to the matter power spectrum through a convolution. From Eqs. (5) and (6) we can write the angular power spectrum as

$$C_l = \int k^2 dk P_v(k) \Delta^2(k), \quad (9)$$

with

$$\Delta^2(k) = \frac{2}{\pi(2l+1)} (l j_{l-1}^2(kx) + (l+1) j_{l+1}^2(kx)). \quad (10)$$

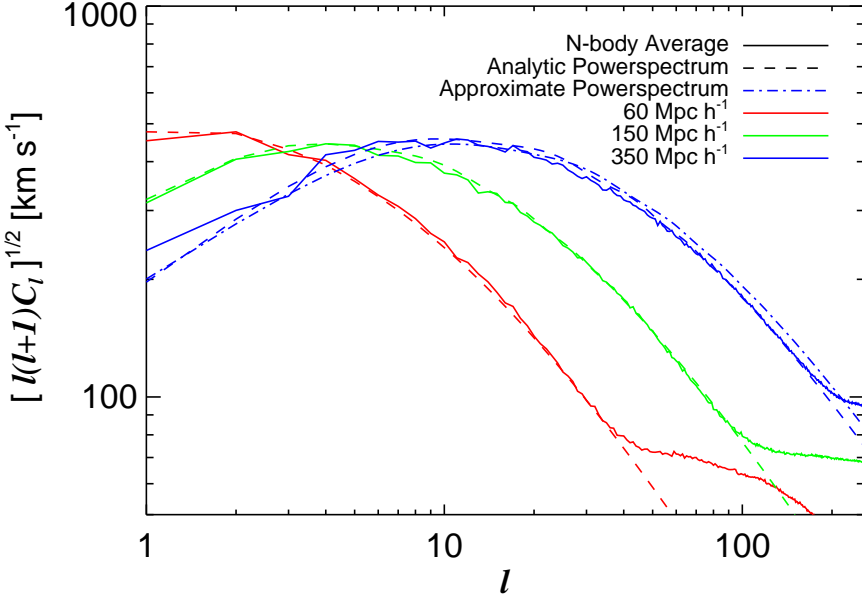


Figure 1. The angular velocity power spectrum at different comoving distances based on an ensemble average from the N-body simulations (full line), and the analytic model (dashed line). The approximation (Eq. 13) to the full analytic model is also shown as the dot-dashed line for $350 h^{-1} \text{ Mpc}$.

Following the approach of [34], the two k -dependent terms in the convolution can be significantly simplified in the limit $l \gg 1$, where the integral is bound from below. The Bessel function is rapidly oscillating, but the envelope has a simple analytic form

$$\Delta_l^2(k) = \begin{cases} \frac{e^2}{8(2l+1)l} \left(\frac{ekx}{2l}\right)^{2(l-1)} \sim 0 & , k < k_* \\ \frac{1}{\pi(kx)^2} & , k \geq k_* \end{cases} \quad (11)$$

$$|W(kR)|^2 = \begin{cases} 1 & , kR < 1 \\ (kR)^{-1} & , kR \geq 1 \end{cases} \simeq \frac{1}{1 + (kR)}, \quad (12)$$

where $k_* = \frac{2}{e}[(2l+1)/l]^{1/2}l/x \simeq \frac{2}{e}(1 - \frac{\ln 2}{2l})l/x$. Collecting terms we find simply

$$C_l = \frac{H^2 f(\Omega)^2}{\pi} \left[\int_{k_*}^{1/R} \frac{dk}{(kx)^2} P_m(k) + \int_{1/R}^{\infty} \frac{dk}{(kx)^2(kR)} P_m(k) \right] \quad (13)$$

A comparison between the exact formula Eq. 5 (the dashed line) and the approximation Eq. 13 (the dot-dashed line) is shown in figure 1, and very good agreement is found. The Bessel function acts like a triangular filter, such that power at a given l only is dependent on scales smaller than $\frac{2}{e}l/x$, and the slow decline of $j_l(kx)^2$ for $\frac{2}{e}k > l/x$ washes out any sharp features and breaks in P_m [34].

In order to get a simple analytic understanding of the behaviour of C_l we use a crude approximation for $P_m(k)$,

$$P_m(k) \sim \frac{Ak}{1+Bk^\alpha}, \quad (14)$$

where $\alpha = 3$ provides a reasonable fit near the maximum of P_m (although not the correct asymptotic limit for $k \rightarrow \infty$). Using this, one finds that for $l \gg 1$

$$C_l \sim \log \left(\frac{x^3 + Bl^3}{Bl^3} \right) = \log(1 + l_0^3/l^3), \quad (15)$$

where $l_0 = x/B^{1/3}$. From this one finds that C_l has a maximum at $l/l_0 = 0.89$ and therefore that the maximum for C_l is proportional to $x/B^{1/3}$. B can be related to the maximum of $P_m(k)$ which is at $k = k_{\max} = 1/(2B^{1/3})$. Therefore the maximum in C_l is directly proportional to the maximum in $P_m(k)$ and the comoving distance x as long as $l_0 \gg 1$.

3.2. Connecting the angular velocity power spectrum with the matter power spectrum

A full-sky supernova sample has both drawbacks and advantages compared with possible galaxy redshift surveys for probing the large scale structure of the universe. The major advantage is that there is no need to know the completeness function of the survey very accurately and that the effective survey volume can be very large using only a relatively small number of objects. However, this also means that it is difficult to probe features on small scales because of the sparseness of the sample. In this regard supernova surveys are fairly similar to surveys like the Sloan Digital Sky Survey Luminous Red Galaxy survey (SDSS-LRG) [35] in which a relatively sparse sample of very bright galaxies is used.

The velocity survey is not affected by bias between baryonic and dark matter, because it is the full matter distribution that sources the velocity field. Together with the lack of sensitivity to completeness it means that supernova velocity surveys are excellent probes of the amplitude of fluctuations, i.e. σ_8 . Given enough statistics they can also be used to probe the shape parameter, Γ , of the matter power spectrum which is related to the α and B parameters in Eq. 14, and to Ω_m (see [36] for a first attempt at probing Γ using present supernova data).

In section 5 we study the sensitivity to σ_8 and Ω_m of mock supernova surveys and find in particular that σ_8 can be very well constrained.

4. Multipole analysis, survey strategy, and construction of mock catalogues

To make a forecast of what can be measured with future supernova catalogues we construct mock catalogues using a refined version of the formalism in [11]. First, we generate a sample with N_{tot} supernovae, and distribute them in a redshift bins. The supernovae are sampled proportionally to density in a large scale N-body simulation (in [11] it was shown that the results are only weakly dependent on the exact distribution

as long as it is semi-random). From this simulated dataset we calculate the angular velocity power spectrum in the different redshift bins from weighted least squares fits of spherical harmonic functions to the radial velocities using the method of singular value decomposition. The multipole expansion is terminated at $l_{max} = \max(\sqrt{N/3}, 20)$, in order to keep the number of degrees of freedom larger than the number of fitted coefficients, $(l_{max} + 1)^2$, (and to keep the solution practical in terms of CPU time).

To get a handle on cosmic variance we repeat the procedure 40 times for differently located observers, and to understand how noise affect the measurement we add a Gaussian noise of $\Delta m = 0.08$ to the magnitude of the supernovae and redo the analysis 900 times per observer.

In figure 1 we show the volume averaged angular power spectrum calculated from the N-body simulation on a thin shell using Healpix [37]. This corresponds to what one would find for an infinitely large supernova sample, assuming that there are no errors on the individual supernovae, and that they all are placed at exactly the same distance.

4.1. The error budget

When comparing the true ensemble averaged angular power spectrum with that derived from a specific finite sample of supernovae, various errors are introduced. There is a *luminosity error* from the combined error in both apparent and absolute magnitudes of the individual supernovae. Then there is a difference between an angular power spectrum, sampled by supernovae in a redshift bin of finite thickness, even in the absence of errors, and the true underlying angular power spectrum. We call it the *geometric error*. It depends only on the specific geometry, or angular distribution, of the supernova sample, and the thickness of the bin. Finally, at low l and small distances the error will be dominated by *cosmic variance* (see figure 2 for a breakdown of the error budget in two specific redshift bins).

To understand the statistical properties, and compensate for the noise, we make two independent set of mock catalogues of observations with different synthetic observers. The first is used to draw mock observers, while the second is used to model the noise, and subtract it from the mock observers. This is done to mimic real observations, where there are no correlations between the observations and the mock catalogues used to model the noise. For each observer in the second set of catalogues we measure the true angular power spectrum, and the angular power spectra derived from a given number of supernovae, with and without noise included. This gives us a robust prediction for the angular power spectra of the luminosity error and the geometric error, as well as the variances on the two types of errors. Comparing volume averaged underlying power spectra from different observers we find the scatter from cosmic variance. In figure 2 we show the three different types of error terms for the three different mock surveys, which will be described in detail below. It can be seen that the luminosity error eventually begins to dominate at high l , while the geometric error is mostly important when considering small number of supernovae. At low l the error from cosmic variance

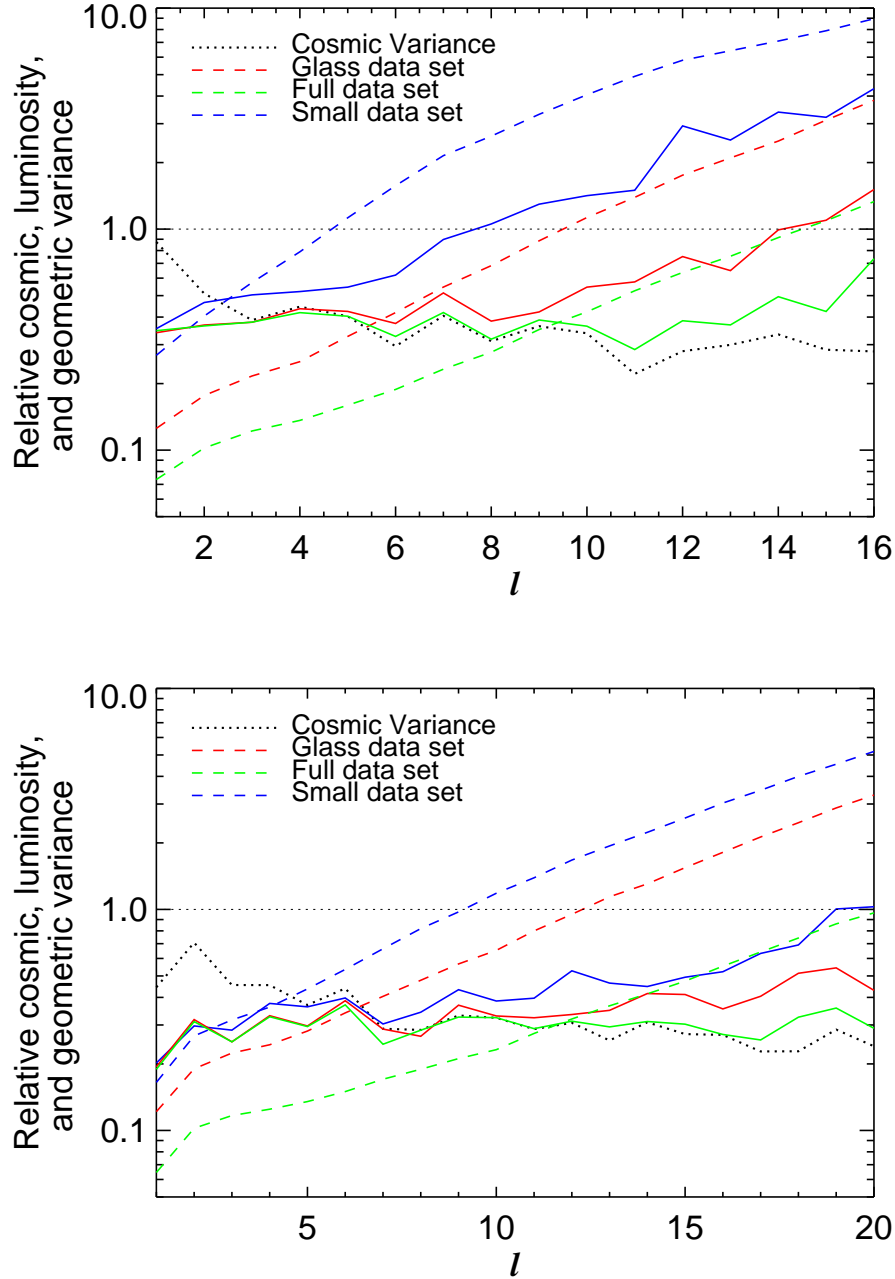


Figure 2. The variances divided by the signal in a redshift bin for the different error terms. The upper (lower) panel is for a bin centered on $100 h^{-1} \text{ Mpc}$ ($150 h^{-1} \text{ Mpc}$). Dashed and full lines are for luminosity and geometric errors respectively, while the thick dotted line is the cosmic variance. The $100 h^{-1} \text{ Mpc}$ bin contains 752 supernovae in the small and glass data sets and 3009 supernovae in the full data set. The corresponding numbers for the $150 h^{-1} \text{ Mpc}$ bin are 1781 and 7125.

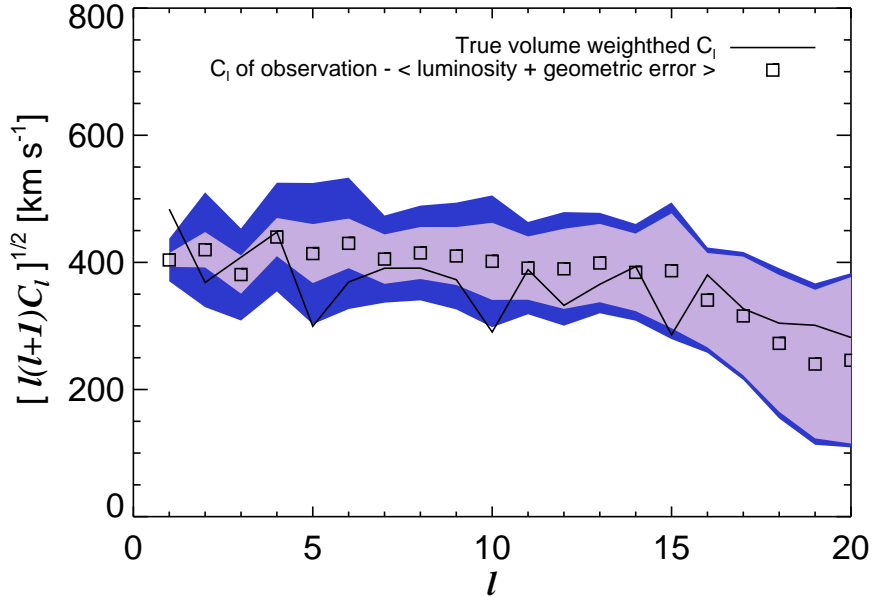


Figure 3. The radial velocity angular amplitude spectrum in a bin centered at a comoving distance of $150 h^{-1}$ Mpc based on a synthetic supernova survey bin with 7125 randomly distributed supernovae. Blue (purple) contours indicate the errors due to the noise correction procedure and including (excluding) cosmic variance with a Gaussian intrinsic and observational scatter of $\Delta m = 0.08$ on each supernova. The full line is the true volume averaged amplitude spectrum for the specific observer, while the squares show the corresponding synthetic observation.

dominates completely, as expected.

4.2. Geometric errors and supernovae on a glass

When considering a mock observation, for very low l the true angular power spectrum can easily be recovered. However, for large l the geometric error is considerable. This phenomenon occurs because there are “holes” in the sky coverage (this is discussed in detail in [11]). These holes lead to leaks of power between different l modes (the spherical harmonics restricted to the positions of the supernovae are no longer orthogonal functions).

As noted in [11] a very important quantity is the size of the largest holes in the distribution of supernovae on the sky. We define a hole at a given point p on the sphere as the largest circle, which can be drawn around that point without encompassing any supernovae. The hole can be quantified in terms of the angle $\theta(p)$ of that sphere. For a random point distribution on the sky the area-averaged size of holes must then be proportional to $N^{-1/2}$ where N is the number of supernovae in a given redshift bin. In figure 4 we show that this relation holds exactly when averaged over many realisations. However, the size of the largest hole drops as roughly $N^{-0.45}$ (as can be seen from figure

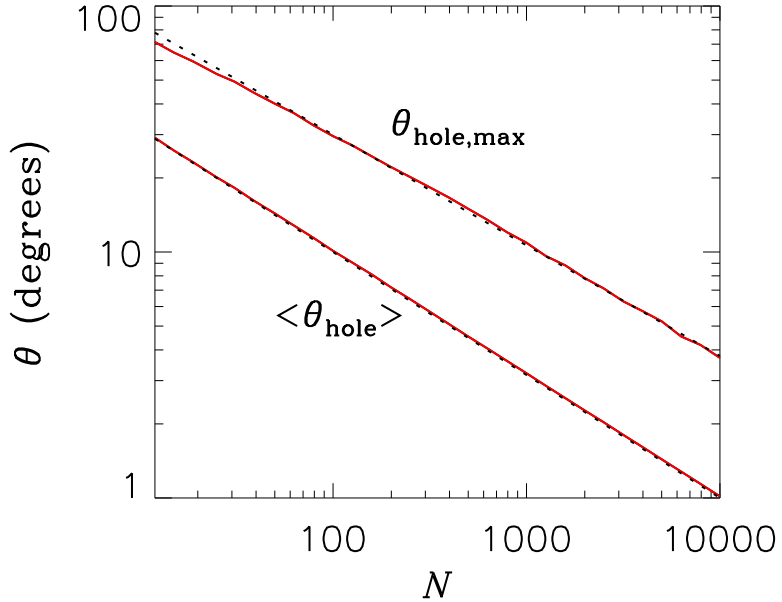


Figure 4. The area-averaged size of holes ($\langle\theta_{\text{hole}}\rangle$), and the size of the largest hole ($\theta_{\text{hole,max}}$) on the sky as a function of the number of supernovae are shown as full (red) lines. Overplotted are dotted lines corresponding to $\langle\theta_{\text{hole}}\rangle \propto N^{-1/2}$ and $\theta_{\text{hole,max}} \propto N^{-0.45}$.

4). In the region of interest this quantity is also a factor 3-4 larger than the average hole size.

Since the largest holes are most problematic in the sense of loss of orthogonality of the spherical harmonics it would be highly desirable with a survey strategy, which attempts to minimise the largest holes rather than the average size of holes. Quantitatively this means a distribution on the sphere, which is as homogeneous as possible for a given number of supernovae.

The survey telescopes supply us with light curves for a set of supernovae, for a subset of host galaxies known redshifts can be found in galaxy catalogues and the literature, and then the question is which of the remaining host galaxies to measure redshifts for, to best reconstruct the radial velocity field. Because we need the redshift of the host galaxy and not the supernova itself, the observing strategy can be decided at a later time when a large sample of supernova have already been observed and the angular distribution is known.

We have tested different geometrical point measurements of radial velocity fields with a known angular power spectrum, and found that a regular homogeneous point distribution, such as a Healpix distribution [37], consistently reconstructs the power spectra with smallest errors. Unfortunately nature is not regular, but given the realities of a semi-random distribution of N supernovae on the sky in each redshift bin to draw from, it is possible to make an almost regular distribution, containing only N_{stop} supernovae, where typically $N_{\text{stop}} \sim N/4$.

To test our algorithm, we have first made mock catalogues of supernovae from an N-

body simulation, by selecting an observer at random, but following the mass distribution; and then selecting N_{tot} supernovae at random. The probability of selecting a given supernova is proportional to the matter density in the bin. Then our algorithm proceeds as follows – applied to the separate redshift bins of the individual mock catalogues:

- A random subset containing N_{start} of the points are drawn from the parent distribution of N supernovae in the redshift bin. They correspond to host galaxies with known redshifts.
- The supernova, outside the subset, with the maximal minimum angular distance to the already selected supernovae is added to the subset (a redshift is measured for the host galaxy of this supernova).
- The last point is iterated adding new supernovae until N_{stop} of the points have been selected.

The resulting distribution is homogeneous but irregular, resembling a glass distribution (see figure 5). The distribution of holes, or, more precisely, the minimum distance from a given point on the sky, to a host galaxy, for a set of glass supernovae, compared to a random set, is characterised by having approximately the same average distance to a supernova, but no big holes in the angular distribution. Using only a quarter of the supernovae, it is competitive with the parent random distribution. (see figure 6, and the variance on the geometric error in figure 2).

4.3. Power spectra derived from a combination of mock observations and catalogues

To estimate how precisely cosmological parameters can be measured we will use three different datasets in the following:

- A “full” dataset containing $N_{tot} = 92,100$ supernovae, distributed randomly according to mass in the N-body simulations. This corresponds to three years of full sky coverage by survey telescopes, with follow up observations on the redshift of all host galaxies. The maximum redshift is $z = 0.13$, corresponding to $400 h^{-1} \text{Mpc}$ and the data is analysed in six redshift bins.
- A “glass” dataset of $N_{tot}/4$ supernovae, constructed from the full dataset using 25% of the supernovae, and the algorithm described above in this section.
- A “small” dataset which contains $N_{tot}/4$ supernovae, distributed according to mass in the N-body simulations.

Using the average power spectra of both the geometric and the luminosity errors to correct the power spectrum of a single mock observation, we are able to probe the power spectrum up to $l_{max} \sim 20$ at distances of $z = 0.03 - 0.13$ (see figure 3) quite robustly, when the full data set is included in the analysis. In figure 7 is shown the equivalent angular power spectra using the glass and the small data set. It is clear that both the overall quality and the systematic of the angular power spectrum are greatly enhanced by using a glass distribution. Notice in figure 2, how the variance in the

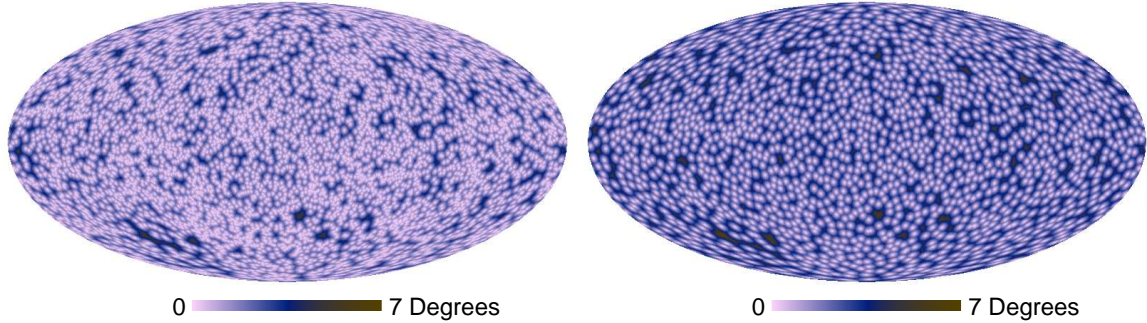


Figure 5. The angular distribution of holes for 7125 random supernovae (left) and for 1781 glass supernovae drawn from the 7125 supernovae using a basis of 445 random supernovae (right). The regular distribution of the glass supernovae is apparent, while the random supernovae follow the underlying density field.

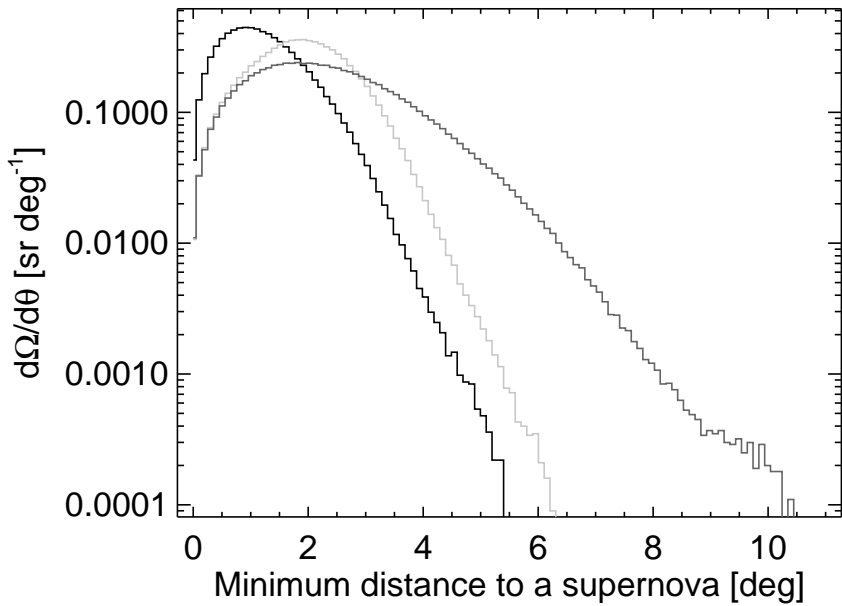


Figure 6. Histogram of the angular distribution of holes for 7125 random supernovae (black curve), 1781 random supernovae (dark grey), and 1781 glass supernovae drawn from the 7125 supernovae (light grey). The number of large holes in the case of a glass distribution is almost the same as for the parent random distribution.

geometric error of the glass supernovae is comparable to that of the parent full data set, and at the same level as cosmic variance, while the variances in both the geometric and the luminosity error from the small set is significantly higher for $l > 8$ and $l > 12$ in the redshift bin centered at $100 h^{-1}$ Mpc and $150 h^{-1}$ Mpc respectively.

It should be noted that the reason why this "glass" distribution works so well is exactly because it is close to being homogeneous, i.e. it has no large holes.

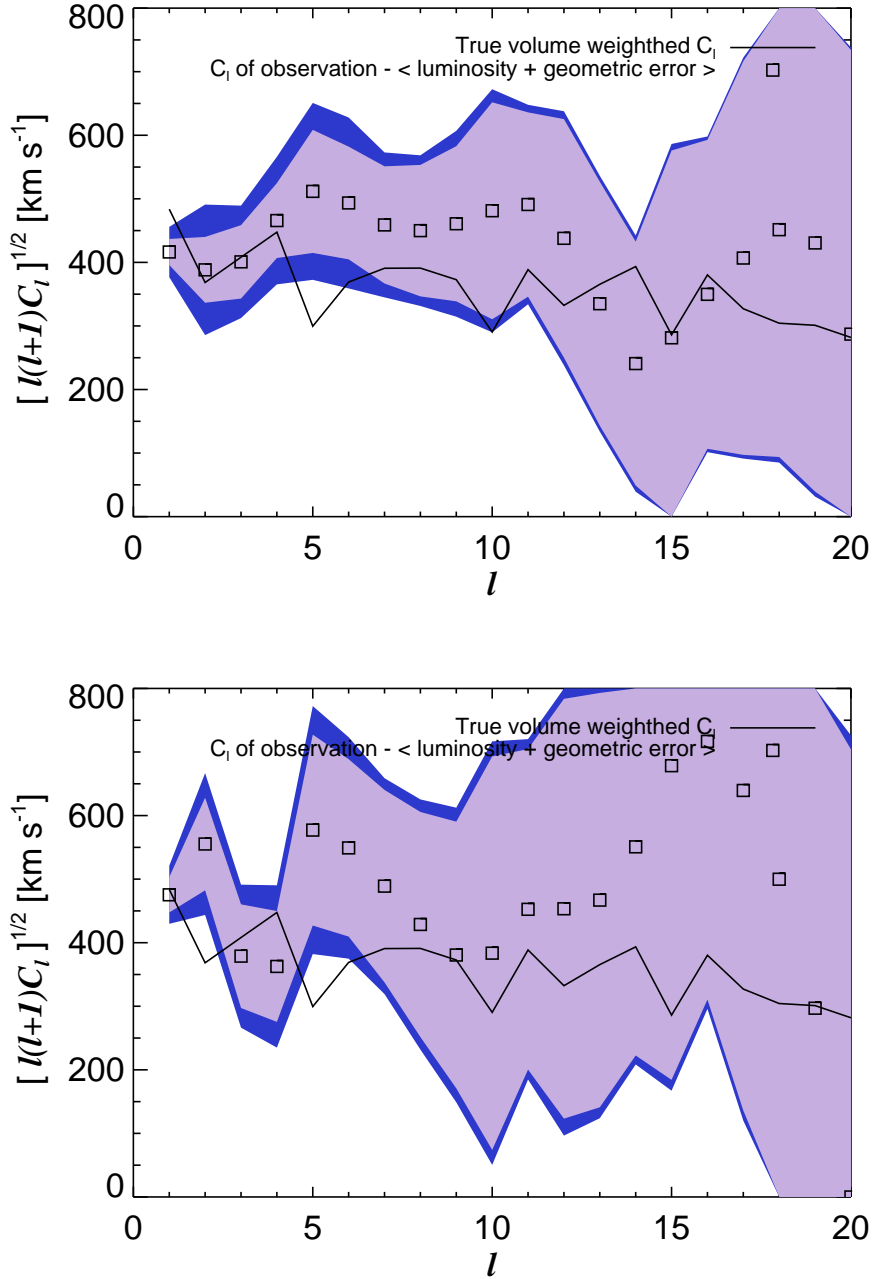


Figure 7. The radial velocity angular amplitude spectrum in a bin centered at a comoving distance of $150 h^{-1}$ Mpc based on a synthetic survey bin with 1781 glass (random) supernovae is shown at the top (bottom). Blue (purple) indicate the errors due to the noise correction procedure and including (excluding) cosmic variance with an estimated luminosity scatter of $\Delta m = 0.08$ on each supernova. The full line is the true volume averaged amplitude spectrum for the specific observer, while the squares show the corresponding synthetic observation.

5. Cosmological parameters

From our mock survey out to $z = 0.13$ we have tested the ability to probe the parameters Ω_m and σ_8 which are directly related to the shape and amplitude of the matter power spectrum around the peak. Specifically we obtained our best model estimate of the observed radial velocity angular power spectrum $C_l^m(\sigma_8, \Omega_m)$, including cosmic variance, geometrical sampling noise, and the luminosity scatter of the supernovae, as the average of 900 supernova mock surveys performed by 40 differently located observers. As the probability density of $|a_{lm}|^2$ is exponential (χ^2 with 2 degrees of freedom) the log likelihood function for a given mock survey within a specific redshift bin is given by

$$-\ln L(\sigma_8, \Omega_m) = \sum_{l=1}^{l_{max}} (2l+1) [\ln C_l^m(\sigma_8, \Omega_m) + C_l/C_l^m(\sigma_8, \Omega_m)] \quad (16)$$

where C_l is the calculated angular power spectrum for the specific redshift shell. The total likelihood function is obtained as the product of the likelihood functions for all redshift bins.

In figure 8 we show 2D contours of the likelihood function based on a fiducial model with $\Omega_m = 0.3$, $\sigma_8 = 0.9$. In figure 9 we show the corresponding 1D likelihood function marginalised over the other parameter.

With the small dataset a precision on σ_8 of roughly 0.06 can be achieved, and with the glass data this is somewhat improved. It should be noted that although the difference between the “small” and the “glass” data sets is quite small in the present case it would be much larger if the intrinsic scatter, Δm , could be reduced, or there were fewer supernovae in the sample. As supernovae become better calibrated standard candles the importance of the “glass” distribution will increase accordingly.

With the full data set the precision is roughly 0.03 at 95% C.L. This is comparable to the estimated precision for Planck+LSST weak lensing [38]. However, we stress that a more thorough parameter study should be performed for the supernova data before a direct comparison can be made with other future probes.

The cosmological parameter estimates can be improved significantly by either reducing the intrinsic scatter, Δm , or increasing the survey volume. Going to $z = 0.2$ is doable in the sense that the changes in apparent magnitude of supernovae are still dominated by peculiar velocities compared to lensing up to fairly large l [17]. In this case the total survey volume will be of order $V \sim 0.9h^{-3}$ Gpc 3 . This is comparable to the SDSS-LRG effective volume of $V \sim 0.75h^{-3}$ Gpc 3 [35] because the supernova survey is full-sky, and the number of objects will be larger than the number of measured LRG galaxies.

6. Discussion

We have performed detailed numerical studies of how future type Ia supernova surveys can be used to probe the large scale velocity field of the local universe out to redshifts $z \sim 0.13$. Our approach was to use high resolution N-body simulations of structure

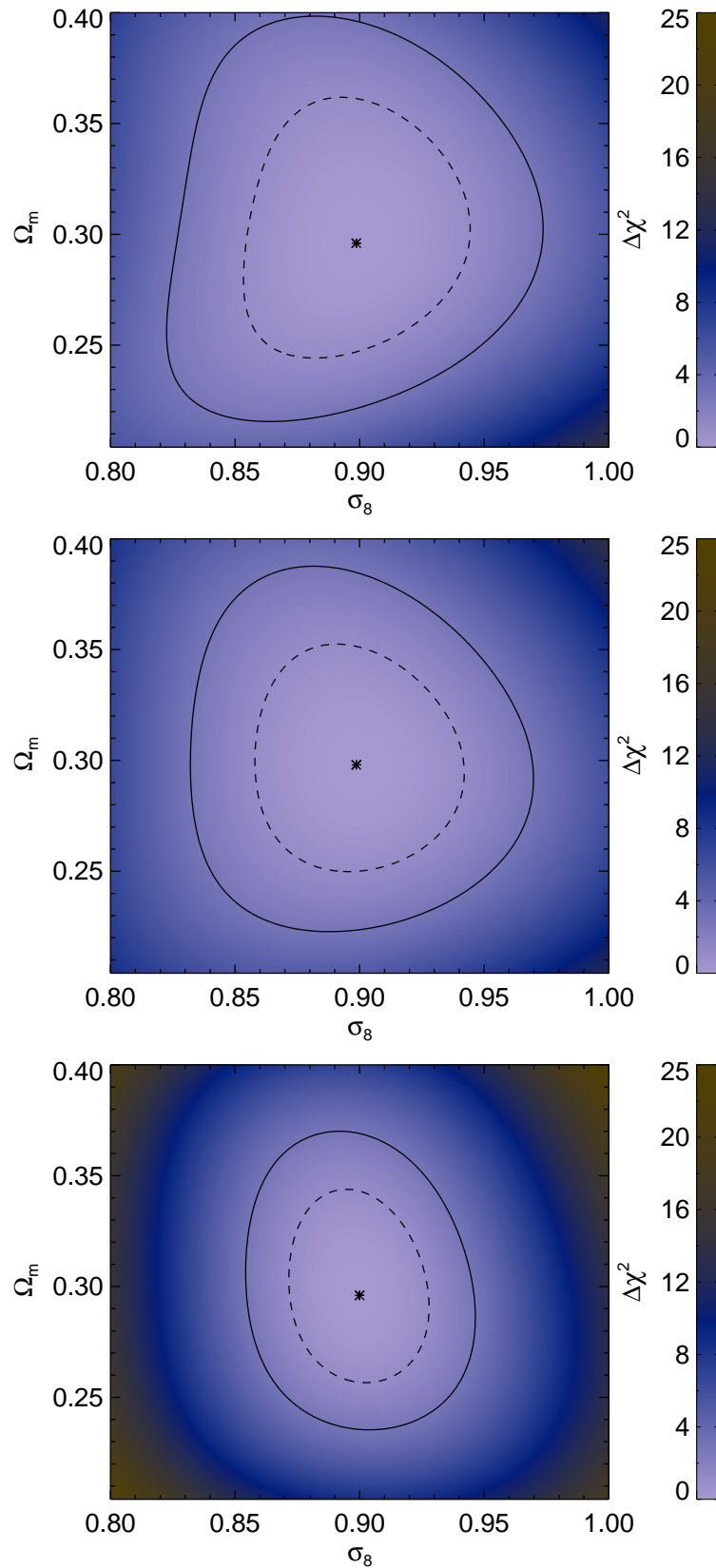


Figure 8. The 2D 68% and 95% C.L. contours for σ_8 and Ω_m for the three synthetic datasets: small (top), glass (middle), and full (bottom).

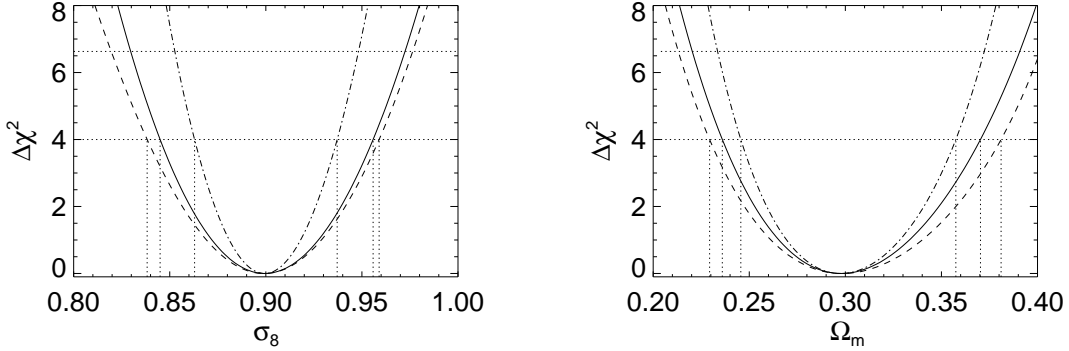


Figure 9. The 1D $\Delta\chi^2$ for Ω_m (left) and σ_8 (right) for the three different datasets.

formation. From these simulations we created many synthetic data sets and used a realistic analysis pipeline to extract the angular velocity power spectrum at different redshifts for each data set.

These velocity power spectra are directly related to the underlying matter power spectrum because the velocity flows are caused by the underlying gravitational potential. Indeed, one of the main advantages of the presently proposed technique is that it directly probes the gravitational potential, unlike galaxy surveys that measure the galaxy power spectrum. This quantity is related to the matter power spectrum only via a scale dependent bias parameter. In this regard future large scale measurements of the velocity power spectrum using type Ia supernovae are similar to the future large scale weak lensing measurements, which also probe the gravitational potential directly. Both probes are complementary to galaxy surveys and combining either with a large scale galaxy survey offers a powerful method for extracting the bias parameter. It will indeed be very interesting to investigate the interplay between future large scale galaxy surveys and supernova surveys in more detail.

Because the velocity power spectrum measured with type Ia supernovae is directly related to the underlying matter power spectrum it is particularly useful for probing the amplitude of fluctuations on scales of a few hundred Mpc, usually quantified by the parameter σ_8 . Using synthetic data sets constructed for different cosmological models we performed a simple likelihood analysis based on a fiducial model with $\Omega_m = 0.3$, $\sigma_8 = 0.9$, and found that σ_8 could realistically be measured with a precision of 3–5% (95% C.L.). This is comparable to the estimated precision of future weak lensing measurements. Furthermore, the precision can be improved significantly by either increasing the survey volume or reducing the intrinsic uncertainty of each supernova.

Much work is still needed in order to accurately gauge the potential of future large scale surveys of low-redshift supernovae for cosmology. However, the present study clearly shows that such surveys, with a relatively small observational effort, can be competitive with other cosmological probes, which will be available in the next decade.

Acknowledgments

We acknowledge many useful discussions with Tamara Davis, Ariel Goobar, and Edvard Mörtsell. We thank the Danish Centre of Scientific Computing (DCSC) for granting the computer resources used. T.H. thanks the Dark Cosmology Centre for hospitality during the course of this work. Some of the results in this paper have been derived using the HEALPix [37] package.

References

- [1] S. Perlmutter et al., 1999, *ApJ*, 517, 565
- [2] B. P. Schmidt, et al., 1998, *ApJ*, 507, 46
- [3] A. G. Riess, et al., 1998, *AJ*, 116, 1009
- [4] J. L. Tonry, et al., 2003, *ApJ*, 594, 1
- [5] R. Knop et al., 2003, *ApJ*, 598, 102
- [6] A. G. Riess, et al., 2004, *ApJ*, 607, 665
- [7] P. Astier et al, 2006, *A&A*, 447, 31
- [8] W. M. Wood-Vasey *et al.*, 2007, arXiv:astro-ph/0701041.
- [9] A. G. Riess *et al.*, 2006, arXiv:astro-ph/0611572.
- [10] C. Bonvin, R. Durrer and M. Kunz, 2006, *Physical Review Letters*, 96, 191302
- [11] T. Haugboelle, S. Hannestad, B. Thomsen, J. Fynbo, J. Sollerman and S. Jha, 2007, arXiv:astro-ph/0612137 [to appear in *Astrophys. J.*]
- [12] L. Hui and P. B. Greene, 2006, *Phys. Rev. D*, 73, 123526
- [13] Jha, S., Riess, A. G., & Kirshner, R. P. 2007, *ApJ*, 659, 122
- [14] J. D. Neill, M. J. Hudson and A. Conley, 2007, arXiv:0704.1654
- [15] L. Wang, arXiv:0705.0368 [astro-ph].
- [16] N. Sugiura, N. Sugiyama and M. Sasaki, 1999, *Prog. of Theoretical Physics*, 101, 903
- [17] C. Bonvin, R. Durrer and M. A. Gasparini, 2006, *Phys. Rev. D*, 73, 023523 [arXiv:astro-ph/0511183].
- [18] J. L. Tonry, J. P. Blakeslee, E. A. Ajhar and A. Dressler, 2000, *ApJ*, 530, 625
- [19] D. J. Radburn-Smith, J. R. Lucey and M. J. Hudson, 2004, *MNRAS*, 355, 1378
- [20] http://www.1sst.org/1sst_home.shtml
- [21] E. Cappellaro, R. Evans and M. Turatto, 1999, *A&A*, 351, 459
- [22] J. D. Neill et al., 2007, astro-ph/0701161
- [23] M. Sullivan et al., 2006, *ApJ*, 648, 868
- [24] W. M. Wood-Vasey, 2004, Ph.D. Thesis, arXiv:astro-ph/0505604
- [25] <http://pan-starrs.ifa.hawaii.edu/public/>
- [26] <http://www.mso.anu.edu.au/skymapper/index.php>
- [27] N. V. Kuznetsova and B. M. Connolly, 2006, arXiv:astro-ph/0609637
- [28] Y. Wang, 2007, *ApJ*, 654, L123
- [29] C. Hernández-Monteagudo, L. Verde, R. Jimenez and D. N. Spergel, 2006, *ApJ*, 643, 598
- [30] P. J. E. Peebles, 1993, Princeton Series in Physics, Princeton, NJ: Princeton University Press, 1993
- [31] P. J. E. Peebles, 1976, *ApJ*, 205, 318
- [32] J. J. Monaghan and J. C. Lattanzio, 1985, *A&A*, 149, 135
- [33] A. Lewis and S. Bridle, 2002, *Phys. Rev. D*, 66, 103511 (2002) [arXiv:astro-ph/0205436].
- [34] O. Elgaroy, S. Hannestad and T. Haugboelle, 2003, *JCAP*, 0309, 008 [arXiv:astro-ph/0306229].
- [35] D. J. Eisenstein *et al.* [SDSS Collaboration], 2001, *AJ*, 122, 2267 [arXiv:astro-ph/0108153].
- [36] R. Watkins and H. A. Feldman, 2007, arXiv:astro-ph/0702751.
- [37] K. M. Gorski et al., 2005, *ApJ*, 622, 759

[38] S. Hannestad, H. Tu and Y. Y. Y. Wong, 2006, JCAP, 0606, 025 [arXiv:astro-ph/0603019].